Chemical Science

ROYAL SOCIETY OF CHEMISTRY

EDGE ARTICLE

View Article Online
View Journal | View Issue

Cite this: *Chem. Sci.*, 2020, **11**, 1404

All publication charges for this article have been paid for by the Royal Society of Chemistry

Received 30th September 2019
Accepted 17th December 2019

DOI: 10.1039/c9sc04926f

rsc.li/chemical-science

Proton-conduction photomodulation in spiropyran-functionalized MOFs with large on–off ratio†

Anemar Bruno Kanj, [a] Abhinav Chandresh, [a] Aaron Gerwien, [b] Sylvain Grosjean, [c] Stefan Bräse,[cde] Yuemin Wang, [a] Henry Dube [b] and Lars Heinke *[a]

Proton conduction in nanopores is important for applications in fuel cells, chemical sensors and information processing devices inspired by nature. Here, we present a nanoporous material, a metal–organic framework (MOF) thin film, allowing photomodulation of the aqueous and alcoholic proton conduction of the guests by almost two orders of magnitude. The MOF film possesses spiropyran groups which undergo reversible UV-light induced isomerization to the merocyanine form, a highly polar, zwitterionic molecule, where the strong binding of the guests to the merocyanine isomer efficiently suppresses the proton conduction. Such materials with photomodulated ionic conduction contribute to the development of advanced, remote-controllable chemical sensors and to switchable devices interfacing with biological systems.

Introduction

Ion, in particular proton, conduction is a widely spread phenomenon in nature,[1] *e.g.* in transmembrane proton pumps[2] and sensory receptors.[3] Moreover, proton conduction is the pivotal process in many advanced applications, like efficient and clean electric energy production by proton-exchange-membrane fuel cells[1,4] or in sensors.[5] Therefore, proton-conducting materials attract particular attention. In addition to the established proton-conducting materials, like perfluorosulfonic acid polymers (like Nafion)[6] and oxides,[7] functional nanoporous materials like metal–organic frameworks, MOFs, are investigated for advanced proton-conduction applications.[8] MOFs are nanoporous solid crystals, composed of metal clusters or ions connected by organic linker molecules.[9] MOFs possess various exclusive properties like high porosities with very large specific surface areas, defined structures and a great chemical and structural variety. The MOF structure can be designed by pre- and postsynthetic methods, enabling various functionalities.[10] In this way, MOF materials with embedded water or other proton-conducting molecules in the pores have been realized with proton conductivities in the range of $\approx 10^{-3}$ to 1 S m^{-1} at room temperature,[8c,11] comparable to the state of the art polymeric materials. In addition to applications in fuel cells,[8c,12] proton-conducting MOFs are investigated for applications in other fields, like in chemical sensors[13] and catalysis.[14] A particular aim in the research for advanced materials is the option of dynamic control of the material's properties. Because light is a fast, usually noninvasive signal for dynamic remote-control with a high spatial resolution, using photo-responsive molecules as functional components attract considerable attention.[15] Such photochromic molecules undergo reversible isomerization when irradiated with light of different wavelengths.

Recently, we presented the first nanoporous material with photoswitchable proton-conduction properties.[16] In this proof-of-principle study, the proton conductivity of the alcoholic and triazole guest molecule was reversibly decreased by 35% as a result of the photoisomerization of the azobenzene pendant to the MOF structure. The effect is based on the increased attractive polar interaction between the proton-conducting guests and the photoswitchable azobenzene moieties, whose dipole moment can be switched between 0 and 3 Debye. A major aim is to increase the on–off ratio from a few ten percent to many orders of magnitude, allowing their application in devices.

Here, we present a photoswitchable crystalline material, a MOF thin film, whose proton-conduction properties can be

[a]*Karlsruhe Institute of Technology (KIT), Institute of Functional Interfaces (IFG), Hermann-von-Helmholtz-Platz 1, 76344 Eggenstein-Leopoldshafen, Germany. E-mail: Lars.Heinke@KIT.edu*

[b]*Ludwig-Maximilians-University Munich, Faculty of Chemistry and Pharmacy, Butenandtstr. 5-13, 81377 München, Germany*

[c]*Karlsruhe Institute of Technology (KIT), Institute of Biological Interfaces 3 – Soft Matter Lab (IBG-3), Hermann-von-Helmholtz-Platz 1, 76344 Eggenstein-Leopoldshafen, Germany*

[d]*Karlsruhe Institute of Technology (KIT), Institute of Organic Chemistry (IOC), Fritz-Haber-Weg 6, 76131 Karlsruhe, Germany*

[e]*Karlsruhe Institute of Technology (KIT), Institute of Biological and Chemical Systems (IBCS-FMS), Hermann-von-Helmholtz-Platz 1, 76344 Eggenstein-Leopoldshafen, Germany*

† Electronic supplementary information (ESI) available. See DOI: 10.1039/c9sc04926f

massively altered. This MOF film, prepared in a layer-by-layer fashion resulting in surface-mounted MOF (SURMOF), possesses photoswitchable spiropyran moieties. Spiropyran[17] is a stimuli-responsive molecule, which may reversibly isomerize to its open merocyanine form upon irradiation with UV light. It is intensively investigated for various applications such as light-responsive glasses[18] and for information storage.[19] Since merocyanine is a zwitterionic molecule, the spiropyran-to-merocyanine isomerization goes along with a change of the dipole moment from about 5 to 16 Debye.[17b] MOFs with spiropyran, attached to the scaffold or embedded in the pores, have been used for photoswitching the color of the material,[20] the uptake amount of the guest molecules[21] as well as the electron (hole) conductivity.[22] For the first time, we take advantage of the large dipole moment change to dramatically modify the MOF properties, here the proton-conductance of the guest molecules. In addition to switching the alcoholic proton conduction, the concept is extended to water, the most important molecule for proton conduction applications. We demonstrate that the aqueous proton conductivity can be photomodulated by two orders of magnitude.

Results and discussion

The surface-mounted metal–organic framework (SURMOF) thin film was prepared on the substrate in a layer-by-layer fashion. The crystallinity of the sample was investigated by X-ray diffraction (Fig. 1). The X-ray diffractogram shows that the film is crystalline with the targeted pillared-layer Cu_2(e-BPDC)$_2$(dabco) structure,[23] where e-BPDC refers to the 2-ethynyl-[1,1′-biphenyl]-4,4′-dicarboxylic acid layer linker and dabco refers to the 1,4-diazabicyclo[2.2.2]octane pillar linker. In addition, the film is grown mainly in [100] direction perpendicular to the substrate surface. Upon incorporating spiropyran in the parent SURMOF by post-synthetic modifications (PSM), the X-ray diffractogram of the sample shows no significant change in the positions and the intensity ratios of the diffraction peaks, indicating that the MOF lattice is unaffected by the PSM process. Noteworthy, the X-ray diffractograms of the sample before and after performing the proton-conduction experiments (including loading with methanol, ethanol and water for 400 min each) are virtually identical (see Fig. 1c). This indicates that the SURMOF is stable under the used conditions.

The reaction yield of the PSM was investigated by infrared spectroscopy (Fig. SI2†). The intensity of the ethynyl vibrational band at 3300 cm^{-1} decreased by 41.5%, which is correlated to the ethynyl groups that underwent ethynyl-azide click reaction anchoring the spiropyran moiety. Since each parent Cu_2(e-BPDC)$_2$(dabco) SURMOF unit cell possesses two ethynyl groups, in average, there are 0.83 photoswitchable moiety anchored in each MOF pore, *i.e.* almost 1 per pore, referred to as Cu_2(SP-BPDC)$_2$(dabco) SURMOF.

The distance between the van der Waals-surfaces of two opposing e-BPDC-linkers is approximately 1.0 nm, which is a measure for the size of the pore and pore window (see Fig. 1b). The total free pore volume of each MOF unit cell is approximately 1.5 nm^3 before the PSM. After PSM (with one spiropyran moiety per pore) the free pore volume of each unit cell decreases to approximately 1.2 nm^3. Since the spiropyran moieties in the pore are flexible and can rotate (or wiggle), *e.g.* around the bonding axis of the linker, the pore diameter and size of the pore window are not strongly affected by the PSM.

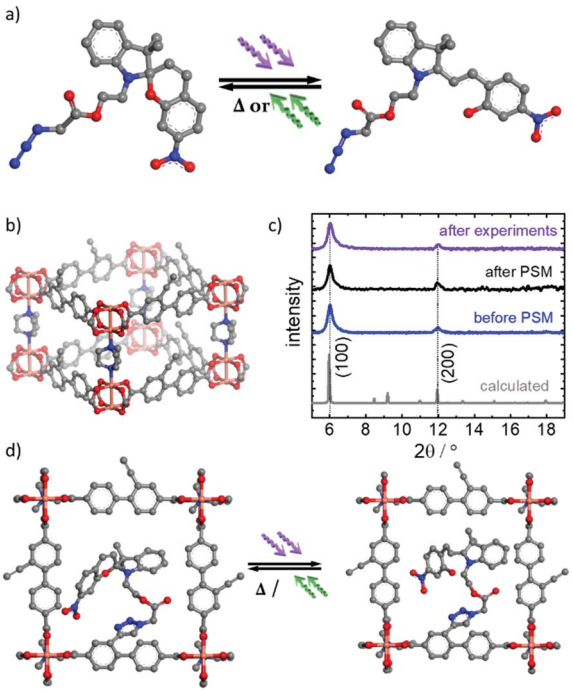

Fig. 1 (a) Photoswitchable spiropyran (left) undergoes isomerization to the merocyanine (right) form upon irradiation with UV light. Isomerization back to the spiropyran form occurs by thermal relaxation or upon irradiation with visible light. (b) The structure of the Cu_2(e-BPDC)$_2$(dabco) parent SURMOF. Copper atoms are shown in orange, oxygen red, nitrogen blue and carbon grey; hydrogen atoms are not shown for clarity. (c) X-ray diffractograms of the pristine Cu_2(e-BPDC)$_2$(dabco) SURMOF grown on interdigitated gold electrodes on glass substrate (blue), after PSM incorporating spiropyran (black), resulting in Cu_2(SP-BPDC)$_2$(dabco) SURMOF, and after the vapor loading and conduction experiments (violet). The grey line shows the calculated powder diffractogram of the structure. The experimentally observed diffraction peaks are labelled. (d) The pore window of Cu_2(SP-BPDC)$_2$(dabco), where the photoswitchable moiety undergoes photoisomerization from spiropyran (left) to merocyanine (right) under irradiation with UV light and back to the spiropyran form upon thermal relaxation or irradiation with visible light.

The photoswitching of the functional molecules is investigated by UV-vis spectroscopy (Fig. 2). The spiropyran-to-merocyanine isomerization of the molecules in ethanolic solution upon UV light irradiation (Fig. 2a) can be seen by the increase of the absorption band at approximately 550 nm. This band is correlated to the merocyanine isomer, being a clear indication of the photoisomerization.[17b,c] The UV irradiation of the Cu_2(SP-BPDC)$_2$(dabco) SURMOF results in the evolution of an absorption band at approximately 580 nm, which is correlated to the merocyanine isomer (Fig. 2b). As a result of the different molecular environment in the SURMOF, the merocyanine absorption band is slightly red shifted in comparison to the absorption band of the ethanolic solution.[17c]

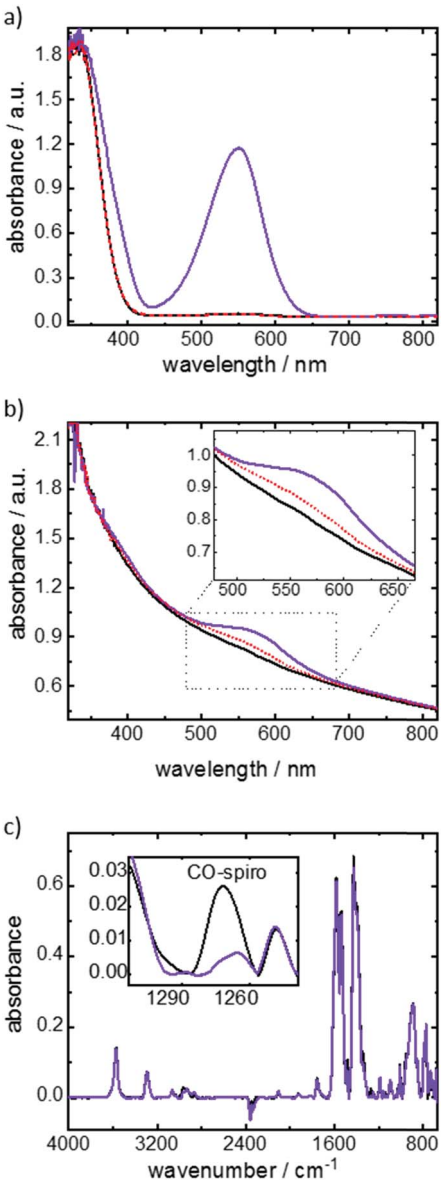

Fig. 2 Spectroscopic investigation of the photoswitching. UV-vis spectra of spiropyran in ethanolic solution (a) and of the Cu_2(SP-BPDC)$_2$(dabco) SURMOF (b). The spectra are: black – pristine, violet – after irradiation with UV light for 25 min and red – after thermal relaxation. (c) Infrared vibrational spectra of the SURMOF sample. The spectrum of the pristine SURMOF is shown in black, the spectrum of the sample upon UV-light irradiation is shown in violet. The zoom-in shows a magnification of the CO-spiro vibration band. Upon UV irradiation, the intensity decreases to 20% of the initial value, thus 80% of the molecules are isomerized from spiropyran to merocyanine.

The photoisomerization is investigated in more details by infrared vibrational spectroscopy. The CO-spiro vibrational band only occurs for the spiropyran isomer and not for the merocyanine form, thus allowing the quantification of the photostationary state (PSS) upon UV irradiation (Fig. 2c). Based on the data, a switching yield of approximately 80% merocyanine was achieved upon 365 nm-UV-light irradiation.

The SEM images (Fig. SI3†) show that the SURMOF homogenously covers the substrate and has a thickness of approximately 0.7 μm.

The ionic conduction properties of the Cu_2(SP-BPDC)$_2$(dabco) SURMOF are investigated by impedance spectroscopy. The empty sample shows a very small conductivity (Fig. SI4†). Upon loading the sample with water from the gas phase, resulting in H_2O@Cu_2(SP-BPDC)$_2$(dabco), the conductivity significantly increases. The analysis of the impedance data in the Nyquist plot (Fig. 3) shows that the non-irradiated H_2O@Cu_2(SP-BPDC)$_2$(dabco) sample, *i.e.* in the spiropyran form, has an ohmic resistance of approximately 3.45 ± 0.5 MΩ. This corresponds to a conductivity of 2.5×10^{-6} S m^{-1}. Upon UV-induced switching to the merocyanine form, the resistance of the H_2O@Cu_2(SP-BPDC)$_2$(dabco) sample increases to 279.5 ± 19 MΩ. This means the spiropyran-to-merocyanine isomerization results to a conductivity decrease by a factor of 82. The conduction switching is fully reversible and the initial Nyquist plot is obtained after thermal relaxation of the photoswitches.

In addition to the aqueous proton conduction, the charge transfer of other common proton-conducting molecules was also investigated. The Nyquist plots of the impedance of ethanol and of methanol loaded in Cu_2(SP-BPDC)$_2$(dabco) SURMOF are shown in Fig. SI5.† Both molecules show strong proton conduction properties in the SURMOF. By UV-light induced spiropyran-to-merocyanine isomerization of the host SURMOF, the ohmic resistance increases by more than one order of magnitude (Fig. SI5†). The resulting proton conductivities of the sample in the spiropyran and merocyanine form are summarized in Fig. 4. It shows that the proton conductivity of

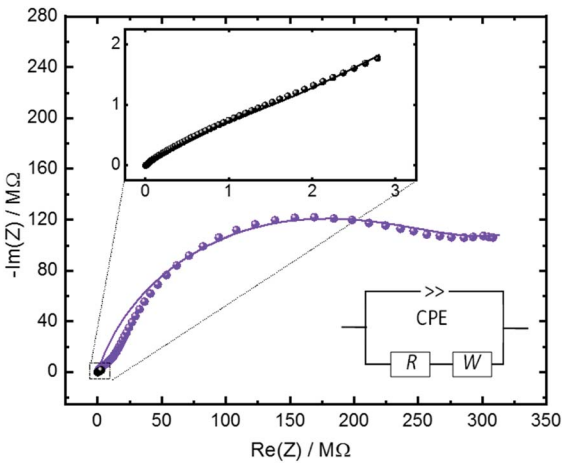

Fig. 3 Nyquist plot of the impedance Z of the H_2O@Cu_2(SP-BPDC)$_2$(dabco) sample in the frequency range from 1 Hz to 5 MHz. The black data are measured for the pristine SURMOF, violet after irradiating the sample with UV light resulting in the isomerization to the merocyanine form. The zoom-in shows a magnification of the data of the sample in the pristine, spiropyran form. The thin lines represent the modelling of the experimental data by the reference circuit, shown in the inset. The circuit, composed of a constant phase element (CPE), ohmic resistance (R) and of Warburg impedance with a 45° phase (W), is a common model to analyse the proton conduction in nanoporous materials.[24] The determined parameters are presented in Table SI1.†

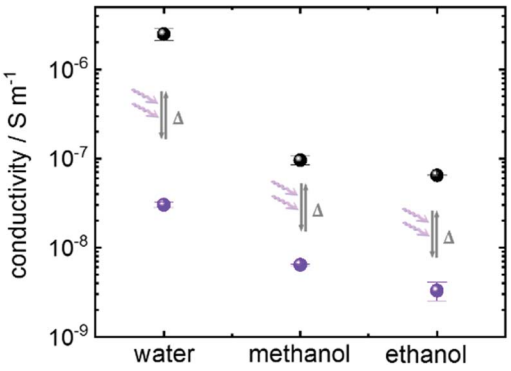

Fig. 4 Conductivity of water, ethanol and methanol in Cu_2(SP-BPDC)$_2$(dabco) SURMOF with the photoswitchable groups in the spiropyran form (black) and in the merocyanine form (violet). The experiments (Fig. 3 and SI5†) are repeated three times. The average values and the standard deviations as error bars are shown here.

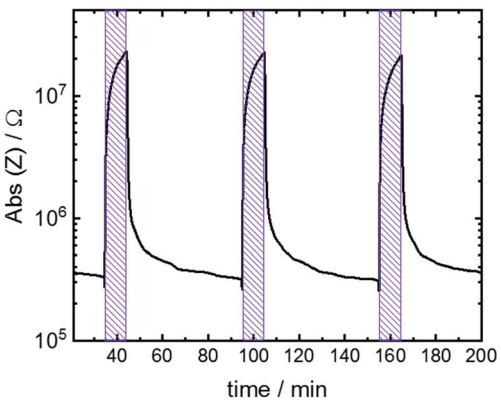

Fig. 5 Absolute value of impedance Z of the H_2O@Cu_2(SP-BPDC)$_2$(dabco) sample at 1 Hz *versus* time. The sample is irradiated with UV light for 10 min each.

all studied guest molecules can be photomodulated by more than one order of magnitude. The highest on–off ratio is reached for aqueous proton conduction.

The time course during the switching of 3 subsequent cycles is shown in Fig. 5. The absolute value of the impedance quickly increases upon starting the UV irradiation, resulting in the spiropyran-to-merocyanine isomerization. Upon 10 min irradiation, the impedance value increased by almost 2 orders of magnitude. After the irradiation, the sample relaxes back to the spiropyran state and the impedance value decreases to its initial value. The data shows that the cycling can be repeated and the behavior is reversible.

The 3 subsequent cycles have similar switching behavior. Thus, prominent photobleaching as previously observed for embedded spiropyran[22] seems to be oppressed. We speculate that the dimerization, which typically leads to the photobleaching of many spiropyran compounds,[17c] is hindered by the anchoring at the MOF scaffold. Note, UV-induced photoconduction processes[25] or significant electronic conduction due to spiropyran-to-merocyanine isomerization,[22] both increasing the conductivity, cannot be observed and have only a negligible influence.

Infrared spectroscopy of the sample loaded with the guests was performed to gain deeper insights into the molecular mechanism of the proton-conduction photomodulation. To distinguish the vibration bands of the guests from the vibrations of the host MOF, D_2O was used as guest molecules. After loading with D_2O, apart from the D_2O band at 2640 cm^{-1}, the corresponding infrared data do not show any significant changes to the empty SURMOF in the spiropyran form (Fig. 6). However, upon UV-light induced spiropyran-to-merocyanine isomerization, a rather broad feature was observed at 1900–2300 cm^{-1}, which is characteristic for the formation of hydrogen bonds.[26] The broadening effect due to strong coupling makes an unambiguous identification of different types of hydrogen bonds (OD···O, OD···N, and ND···O) extremely difficult. Note, such hydrogen bonds are also not observed for the empty merocyanine-SURMOF (see Fig. 2c). The assignment of the hydrogen bonds is further supported by the observation of H_2O-related hydrogen bonding at the high-frequency range. As shown in Fig. 6, a broad IR feature appeared at 2800–3300 cm^{-1}, which are typical for the hydrogen-bonded O–H and N–H stretching vibrations. Overall, the present IR results provide direct spectroscopic evidence that water guest molecules are strongly adsorbed *via* hydrogen-bonding formed only in the presence of the merocyanine-SURMOF.

Based on the small pore size, we tentatively assume that the proton conduction follows the Grotthuss mechanism.[27] The alignment of the water molecules, which allow relatively efficient Grotthuss-like proton transfer in the spiropyran-SURMOF, is disturbed by the strong hydrogen-bonding to the merocyanine-SURMOF, resulting in a substantially decreased proton mobility and, hence, in the smaller proton conductivity of water. These results are in agreement with previous infrared vibrational spectroscopy and density-functional theory calculation of butanediol and triazole in azobenzene-containing SURMOFs.[16] It should be note that a dense hydrogen-bond network generally would favor efficient, long-range proton transport,

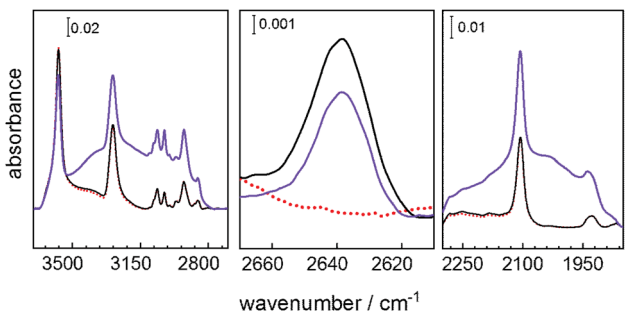

Fig. 6 Infrared spectra of the Cu_2(SP-BPDC)$_2$(dabco) SURMOF. The spectrum of the empty SURMOF is shown as red dotted line, the D_2O-loaded SURMOF in the spiropyran form is shown as black solid line and in the merocyanine form as violet line. The center panel shows the band of D_2O valence vibration. The panel on the right- and left-hand side show the vibration of the H-bonded and D-bonded species. The entire infrared spectra are shown in Fig. SI6.†

which is in contrast to the experimental findings. In addition, the MOF, in both spiropyran and merocyanine forms, contains no ionizable protons. Both findings support the fact that the proton-conduction-change results not from changes in hydrogen-bond networks but from the strong short-range binding of the guests.

The presented MOF with spiropyran moieties shows a tremendously larger switching effect in comparison to state-of-the-art photoswitchable MOFs, namely MOFs with azobenzene moieties.[16] Since the modulation of aqueous proton conduction was not yet published, we compare the proton-conduction of alcohol guest molecules. While the conductivity of butanediol in azobenzene-MOFs is switched only by a factor of 1.5 (corresponding to a decrease by 35%),[16] the conductivity of ethanol in spiropyran-MOFs is photomodulated by a factor of 20. The 13-times-higher switching effect is explained by the different dipole moment changes of the photoswitchable components. While the dipole moment μ of azobenzene changes only from 0 D (*trans*) to 3 D (*cis*), the dipole moment of spiropyran changes approximately from 5 D (spiropyran form) to 16 D (merocyanine form). The substantially larger dipole moment of merocyanine results in much stronger hydrogen bonds in comparison to the rather weak hydrogen bonds in the *cis*-azobenzene-MOF. As rough estimation of the bond-strength-changes using Keesom dipole–dipole interaction with $E \sim \mu^2$ (ref. 28) (and disregarding any further interaction of the guests with the host framework as well as the structural differences), the energy change in the spiropyran-MOF is 26 times larger than in the azobenzene-MOF. This value is in the same order of magnitude as the observed proton-conduction-photomodulation difference.

Experimental section

SURMOF synthesis

The thin MOF films, referred to as surface-mounted MOFs (SURMOFs),[29] were prepared in a layer-by-layer fashion in a two-step process. First, the parent MOF thin film with a pillared-layer structure of type Cu_2(e-BPDC)$_2$(dabco) was prepared, where e-BPDC refers to 2-ethynyl-[1,1′-biphenyl]-4,4′-dicarboxylic acid[23b] and dabco refers to 1,4-diazabicyclo(2.2.2)octan. The sample was synthesized by alternative immersion in the synthesis solutions, *i.e.* ethanolic 1 mM copper acetate solution and ethanolic 0.2 mM e-BPDC and dabco solution. The synthesis was performed by 100 cycles using a dipping robot.[30]

By post-synthetic modifications (PSM), the light-responsive spiropyran moieties, *i.e.* 2-(3′,3′-dimethyl-6-nitrospiro[chromene-2,2′-indolin]-1′-yl)ethyl 2-azidoacetate (Fig. 1a and SI1†), were anchored in the MOF pores by ethynyl-azide click reactions,[23b,31] resulting in Cu_2(SP-BPDC)$_2$(dabco) (Fig. 1d). PSM was carried out by immersing the SURMOF in the reaction solution of spiropyran in toluene with a concentration of 3 g per L for 24 hours at room temperature. After the initial immersion, the temperature of the solution was increased to 80 °C for 9 days. Afterwards the sample was rinsed thoroughly with toluene and acetone to remove residual reactants.

Sample characterization

XRD. X-ray diffraction (XRD) measurements in out-of-plane geometry with a wavelength of $\lambda = 0.154$ nm were carried out using a Bruker D8-Advance diffractometer equipped with a position-sensitive detector in θ–θ geometry.

UV-vis spectroscopy. The UV-vis transmission spectra were recorded by means of a Cary5000 spectrometer equipped with a UMA unit from Agilent. The spiropyran solution (Fig. 2a) had a concentration of 0.05 mg per ml and the cuvette thickness is 10 mm.

SEM. Scanning electron microscopy (SEM) images were recorded with a TESCAN VEGA3 tungsten heated filament scanning electron microscope. To avoid charging effects, the samples were coated with a thin (~2 nm) platinum film using a LEICA EM ACE600 device.

Light irradiation. The samples were illuminated with a 365 nm-LED from PrizMatix with a power of about 40 mW cm^{-2}.

IRRAS. The infrared spectra were recorded with a Fourier-Transform Infrared Reflection Absorption Spectrometer (FT-IRRAS) Bruker Vertex 80. The spectra were recorded in grazing incidence reflection mode at an angle of incidence of 80° relative to the surface normal.

Measurement of proton conduction properties

For the conduction measurements, interdigitated gold electrodes with a gap width of 10 μm and a total gap length of 1.69 m deposited on a quartz glass plate were used as SURMOF substrates. These substrates were purchased from Metrohm. The impedance spectra were measured using a Zurich Instruments MFIA Impedance Analyzer for a frequency range of 5 MHz to 1 Hz. The sample was placed in a home-made cell where the interdigitated gold electrodes on the substrate were contacted in a 2-probe way. The amplitude of the electric field between the interdigitated electrodes is approximately 0.03 V μm^{-1}. The cell was purged with pure nitrogen or with nitrogen enriched with the vapor of the guest molecules with a flow rate of 100 ml min^{-1}. The water vapor had a relative humidity of 93%, corresponding a vapor pressure of 29 mbar. The vapor pressure of ethanol and methanol were approximately 75 mbar and 160 mbar, respectively. All experiments were performed at room temperature (298 K). Further details on the setup can be found in ref. 16. All conduction experiments were performed 3 times. The arrhythmic average value and the standard deviation is presented.

Conclusions

A nanoporous metal–organic framework (MOF) thin film with photoswitchable spiropyran moieties is presented and the aqueous and alcoholic proton conduction of the guest molecules is investigated. As a result of the UV-light-induced reversible spiropyran-to-merocyanine isomerization in the host MOF, the bonding strength of the guest to the framework is substantially increased, decreasing their mobility. As a result, the proton conductivity of the guest is photomodulated by up to two orders of magnitude.

The study shows that by using more appropriate photoswitches than azobenzene, which is used for many proof-of-principle photoswitchable-MOF demonstrations,[32] the switching performance can be significantly increased. Such materials with massively photomodulatable proton-conduction may find application in switchable sensors[33] and allow the remote control of the interface to biological materials, in particular to ion conduction channels.[34] We foresee that further functionalization increasing the dipole moment of the photoswitch as well as MOF structure optimization will further increase the conduction on–off ratio.

Conflicts of interest

There are no conflicts to declare.

Acknowledgements

The authors gratefully acknowledge funding by the Volkswagen Foundation, the Fonds der Chemischen Industrie and the German Science Foundation (DFG HE 7036/5).

References

1 K. D. Kreuer, *Chem. Mater.*, 1996, **8**, 610–641.
2 S. Buschmann, E. Warkentin, H. Xie, J. D. Langer, U. Ermler and H. Michel, *Science*, 2010, **329**, 327–330.
3 (*a*) B. Lindemann, *Physiol. Rev.*, 1996, **76**, 719–766; (*b*) D. M. Starace and F. Bezanilla, *Nature*, 2004, **427**, 548–553.
4 (*a*) Y. Wang, K. S. Chen, J. Mishler, S. C. Cho and X. C. Adroher, *Appl. Energy*, 2011, **88**, 981–1007; (*b*) B. C. H. Steele and A. Heinzel, *Nature*, 2001, **414**, 345–352.
5 (*a*) M. R. Karim, K. Hatakeyama, T. Matsui, H. Takehira, T. Taniguchi, M. Koinuma, Y. Matsumoto, T. Akutagawa, T. Nakamura, S. Noro, T. Yamada, H. Kitagawa and S. Hayami, *J. Am. Chem. Soc.*, 2013, **135**, 8097–8100; (*b*) B. Musset, S. M. E. Smith, S. Rajan, D. Morgan, V. V. Cherny and T. E. DeCoursey, *Nature*, 2011, **480**, 273–277; (*c*) G. Alberti, M. Casciola and R. Palombari, *J. Membr. Sci.*, 2000, **172**, 233–239.
6 C. H. Park, C. H. Lee, M. D. Guiver and Y. M. Lee, *Prog. Polym. Sci.*, 2011, **36**, 1443–1498.
7 K. D. Kreuer, *Annu. Rev. Mater. Res.*, 2003, **33**, 333–359.
8 (*a*) C. H. Wang, X. L. Liu, N. K. Demir, J. P. Chen and K. Li, *Chem. Soc. Rev.*, 2016, **45**, 5107–5134; (*b*) S. Horike, D. Umeyama and S. Kitagawa, *Acc. Chem. Res.*, 2013, **46**, 2376–2384; (*c*) M. Yoon, K. Suh, S. Natarajan and K. Kim, *Angew. Chem., Int. Ed.*, 2013, **52**, 2688–2700; (*d*) J. A. Hurd, R. Vaidhyanathan, V. Thangadurai, C. I. Ratcliffe, I. L. Moudrakovski and G. K. H. Shimizu, *Nat. Chem.*, 2009, **1**, 705–710.
9 (*a*) H. Furukawa, K. E. Cordova, M. O'Keeffe and O. M. Yaghi, *Science*, 2013, **341**, 1230444; (*b*) S. Kaskel, *The Chemistry of Metal-Organic Frameworks: Synthesis, Characterization, and Applications*, Wiley, 2016.
10 Z. Q. Wang and S. M. Cohen, *Chem. Soc. Rev.*, 2009, **38**, 1315–1329.
11 S. Pili, S. P. Argent, C. G. Morris, P. Rought, V. Garcia-Sakai, I. P. Silverwood, T. L. Easun, M. Li, M. R. Warren, C. A. Murray, C. C. Tang, S. H. Yang and M. Schroder, *J. Am. Chem. Soc.*, 2016, **138**, 6352–6355.
12 S. L. Li and Q. Xu, *Energy Environ. Sci.*, 2013, **6**, 1656–1683.
13 S. S. Bao, N. Z. Li, J. M. Taylor, Y. Shen, H. Kitagawa and L. M. Zheng, *Chem. Mater.*, 2015, **27**, 8116–8125.
14 N. Reimer, B. Bueken, S. Leubner, C. Seidler, M. Wark, D. De Vos and N. Stock, *Chem.–Eur. J.*, 2015, **21**, 12517–12524.
15 (*a*) B. L. Feringa and W. R. Browne, *Molecular Switches*, Wiley, 2011; (*b*) M.-M. Russew and S. Hecht, *Adv. Mater.*, 2010, **22**, 3348–3360.
16 K. Müller, J. Helfferich, F. L. Zhao, R. Verma, A. B. Kanj, V. Meded, D. Bléger, W. Wenzel and L. Heinke, *Adv. Mater.*, 2018, **30**, 1706551.
17 (*a*) E. Fischer and Y. Hirshberg, *J. Chem. Soc.*, 1952, 4522–4524; (*b*) R. Klajn, *Chem. Soc. Rev.*, 2014, **43**, 148–184; (*c*) L. Kortekaas and W. R. Browne, *Chem. Soc. Rev.*, 2019, **48**, 3406–3424.
18 R. A. Evans, T. L. Hanley, M. A. Skidmore, T. P. Davis, G. K. Such, L. H. Yee, G. E. Ball and D. A. Lewis, *Nat. Mater.*, 2005, **4**, 249–253.
19 D. A. Parthenopoulos and P. M. Rentzepis, *Science*, 1989, **245**, 843–845.
20 H. A. Schwartz, S. Olthof, D. Schaniel, K. Meerholz and U. Ruschewitz, *Inorg. Chem.*, 2017, **56**, 13100–13110.
21 K. Healey, W. B. Liang, P. D. Southon, T. L. Church and D. M. D'Alessandro, *J. Mater. Chem. A*, 2016, **4**, 10816–10819.
22 S. Garg, H. Schwartz, M. Kozlowska, A. B. Kanj, K. Müller, W. Wenzel, U. Ruschewitz and L. Heinke, *Angew. Chem., Int. Ed.*, 2019, **58**, 1193–1197.
23 (*a*) T. Truong, K. D. Nguyen, S. H. Doan and N. T. S. Phan, *Appl. Catal., A*, 2016, **510**, 27–33; (*b*) Z. Wang, J. Liu, S. Grosjean, D. Wagner, W. Guo, Z. Gu, L. Heinke, H. Gliemann, S. Bräse and C. Wöll, *ChemNanoMat*, 2015, **1**, 338–345; (*c*) P. V. Dau and S. M. Cohen, *CrystEngComm*, 2013, **15**, 9304–9307.
24 (*a*) A. Lasia, *Electrochemical Impedance Spectroscopy and its Applications*, Springer New York, New York, NY, 2014; (*b*) R. Abazari, S. Sanati, A. Morsali, A. M. Z. Slawin, C. L. Carpenter-Warren, W. Chen and A. Zheng, *J. Mater. Chem. A*, 2019, **7**, 11953–11966; (*c*) S. Shalini, V. M. Dhavale, K. M. Eldho, S. Kurungot, T. G. Ajithkumar and R. Vaidhyanathan, *Sci. Rep.*, 2016, **6**, 32489.
25 X. Liu, M. Kozlowska, T. Okkali, D. Wagner, T. Higashino, G. Brenner-Weiß, S. M. Marschner, Z. Fu, Q. Zhang, H. Imahori, S. Bräse, W. Wenzel, C. Wöll and L. Heinke, *Angew. Chem., Int. Ed.*, 2019, **58**, 9590–9595.
26 (*a*) Y. M. Wang and C. Wöll, *Chem. Soc. Rev.*, 2017, **46**, 1875–1932; (*b*) H. Noei, F. Gallino, L. Jin, J. Zhao, C. Di Valentin and Y. Wang, *Angew. Chem., Int. Ed.*, 2013, **52**, 1977–1981.
27 S. S. Park, A. J. Rieth, C. H. Hendon and M. Dinca, *J. Am. Chem. Soc.*, 2018, **140**, 2016–2019.

28 (*a*) V. Magnasco, M. Battezzati, A. Rapallo and C. Costa, *Chem. Phys. Lett.*, 2006, **428**, 231–235; (*b*) W. H. Keesom, *KNAW Proc.*, 1915, **18 I**, 636–646.
29 (*a*) O. Shekhah, H. Wang, S. Kowarik, F. Schreiber, M. Paulus, M. Tolan, C. Sternemann, F. Evers, D. Zacher, R. A. Fischer and C. Wöll, *J. Am. Chem. Soc.*, 2007, **129**, 15118–15119; (*b*) L. Heinke and C. Wöll, *Adv. Mater.*, 2019, **31**, 1806324.
30 Z.-G. Gu, A. Pfriem, S. Hamsch, H. Breitwieser, J. Wohlgemuth, L. Heinke, H. Gliemann and C. Wöll, *Microporous Mesoporous Mater.*, 2015, **211**, 82–87.
31 M. A. Gotthardt, S. Grosjean, T. S. Brunner, J. Kotzel, A. M. Gaenzler, S. Wolf, S. Braese and W. Kleist, *Dalton Trans.*, 2015, **44**, 16802–16809.
32 R. Haldar, L. Heinke and C. Wöll, *Adv. Mater.*, 2019, 1905227.
33 J. Zhang, Q. Zou and H. Tian, *Adv. Mater.*, 2013, **25**, 378–399.
34 M. M. Lerch, M. J. Hansen, G. M. van Dam, W. Szymanski and B. L. Feringa, *Angew. Chem., Int. Ed.*, 2016, **55**, 10978–10999.